pendence should also be tested in a differential rather than in an integral manner.

Two last experimental facts are worthy of mention. One is that bombardments of copper and lead targets show that the number of fast deuterons increases with atomic number less rapidly than the number of fast protons.[1] This may be an indication that the pick-up process is more confined to the surface of the nucleus than is a knock-out process. The second fact is that fast tritons have also been observed with perhaps one-tenth the probability of deuterons. If the pick-up hypothesis is correct, more complicated rearrangements are expected also to occur, but, of course, less often.

The authors wish to thank Professors Serber and Wick for helpful theoretical discussions. We are also grateful to H. York and K. Brueckner for their aid in interpreting the experiments. Work described in this report was performed under the auspices of the AEC.

PHYSICAL REVIEW VOLUME 77, NUMBER 4 FEBRUARY 15, 1950

X-Ray and Gamma-Ray Reflection Properties from 500 X Units to Nine X Units of Unstressed and of Bent Quartz Plates for Use in the Two-Meter Curved-Crystal Focusing Gamma-Ray Spectrometer*

D. A. LIND, W. J. WEST,† AND J. W. M. DUMOND
California Institute of Technology, Pasadena, California
(Received October 6, 1949)

The x-ray and gamma-ray reflection properties of the (310) planes of quartz have been investigated over the wave-length range 500 to 9 x.u. for the Laue or transmission case. The plates were inhomogeneously stressed by bending to a cylinder with a radius of 200 cm. The value of the integrated reflection coefficient was deduced from the luminosity properties of the curved-crystal spectrometer for seven different wave-lengths. The data indicate that the integrated reflection coefficient R_θ for a bent crystal varies as λ^2 over the range of wave-lengths studied. This behavior is in accord with that of a mosaic crystal. The reflection properties of the (310) planes of an unstressed crystal plate cut from the same sample were measured over the range 700 to 120 x.u. by the two-crystal spectrometer technique. These results indicate that the unstressed quartz plates behave more nearly as perfect crystals. Data are given on the integrated reflection coefficient, the peak value of Laue reflection coefficient, and the width at half-maximum of the diffraction curve for the unstressed case.

INTRODUCTION

DURING the development of the curved-crystal gamma-ray spectrometer,[1] it became apparent that a careful determination of the reflection properties of the (310) planes of the elastically curved-quartz plates used in the spectrometer would have to be made. At the same time, a thorough analysis of the intensity problem of the spectrometer was carried out. This analysis showed that the determination of the integrated Laue reflection coefficient of the curved crystal was possible from the experimental reflection properties.

While this determination is of particular interest for the design and operation of the curved-crystal spectrometer, it has additional importance because, in the past, other observers[2,3] have noted that the x-ray reflections from inhomogeneously stressed quartz plates show rather marked anomalies not present in unstressed or homogeneously stressed plates. Our experimental results confirm these qualitative observations but, in addition, we offer some quantitative data which may be useful for interpreting the observations.

THEORY

The theory of x-ray diffraction has been completely worked out for a great many conditions. From the character of the diffraction it is possible to deduce some information concerning the perfection of the lattice structure and the nature of its imperfections. A perfect lattice is one in which there exist no disorders of any kind in the atomic arrangement throughout the complete crystal. A mosaic structure, on the other hand, is one in which disorders do exist. It is convenient to describe a mosaic crystal as consisting of small domains each with perfect internal lattice structure which are more or less disarranged in the macroscopic crystal. The essential effect of the domain structure is to cause the scattering from separate domains to be incoherent. For the perfect crystals, two cases are of interest. A "thick" crystal is one for which the primary extinction distance is much smaller than the thickness of the crystal; a "thin" crystal is one for which the extinction distance is much greater than the thickness of the crystal. In a mosaic crystal, the situation is somewhat

* This work was supported by funds supplied through the joint cooperation of the ONR and AEC.
† Now with California Research Corporation, La Habra, California.
[1] J. W. M. DuMond, Rev. Sci. Inst. **18**, 626 (1947).
[2] Y. Sakisaka and I. Sumato, Proc. Phys. Math. Soc. Japan III **13**, 211 (1931).
[3] C. S. Barrett and C. E. Howe, Phys. Rev. **39**, 889 (1932).

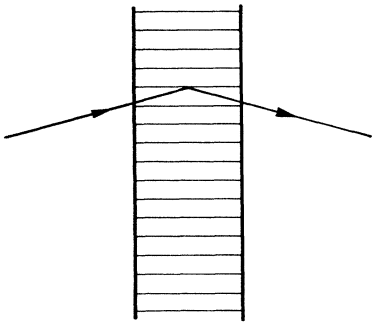

FIG. 1. This figure shows the orientation of the crystal planes and the incident and diffracted beams for the symmetrical Laue case.

more complicated because there are two types of extinction, primary and secondary. "Primary" refers to extinction in the individual mosaic units while "secondary" refers to the extinction which occurs in the macroscopic crystal. The "dynamical theory" of x-ray reflection has been developed first by Darwin[4] and later by Ewald[5] and von Laue.[6] The details of the scattering behavior of real crystals have been given by Zachariasen[7] who follows the developments of Ewald and of Von Laue. The cases which are of most interest for this work are: (1) Negligible primary extinction in the coherent domains and small secondary attenuation in the crystal plate, (2) large primary extinction but small secondary attenuation.

In the curved-crystal spectrometer used at short wave-lengths, only the Laue or transmission case is employed because it is possible thus to realize much greater luminosity than with the Bragg or reflection case. The results of the dynamical theory of x-ray reflection have been completely worked out for these cases.[4,5] It is of interest to examine the theoretical results to see what may be expected when the range of wave-lengths is extended down to wave-lengths of the order of 10 x.u., for at short wave-lengths the effects of much smaller lattice imperfections manifest themselves. The theory leads us to expect that such small lattice imperfections will be masked at longer wave-lengths where the diffraction pattern for an ideal crystal is broader than the angular disturbances in question.

In what follows, the (310) planes of the quartz crystal lay very nearly normal to the plane of the 1-mm thick crystalline slab (symmetrical Laue case), see Fig. 1. The discussion which follows refers therefore to the particular geometry which was employed, namely, that of the symmetrical Laue case exclusively.

[4] C. G. Darwin, Phil. Mag. **27**, 325 (1914); **27**, 675 (1914).
[5] P. P. Ewald, Ann. d. Physik **54**, 519 (1917); **54**, 577 (1917); Zeits. f. Physik **2**, 232 (1920); **30**, 1 (1924); Physik. Zeits. **26**, 29 (1925).
[6] M. von Laue, Ergeb. d. exakt. Naturwiss. Bd. X, 137–158 (1931); *Rontgenstrahl-interferenzen* (Akademische Verlagsgesellschaft, Leipzig, 1941).
[7] W. H. Zachariasen, *Theory of X-Ray Diffraction in Crystals* (John Wiley and Sons, Inc., New York, 1945).

The rigorous development of the dynamical theory of x-ray reflection tends to obscure rather than reveal the physical interpretation. We, therefore, here give a brief non-rigorous physical argument leading to the required results.

The Ewald construction (Fig. 2) of the propagation sphere inside the crystal lattice serves to determine the allowable propagation vectors. Except for the dispersion effects‡ the Bragg equation must be satisfied,

$$\mathbf{k}_H - \mathbf{k}_0 = 2\pi \mathbf{B}_H. \tag{1}$$

The Ewald construction is the graphical representation of Eq. (1). $\mathbf{k}_H$, $\mathbf{k}_0$ are propagation vectors outside the crystal for the diffracted and incident beams, respectively, and have identical magnitudes $2\pi/\lambda$; $\mathbf{B}_H$ is a vector of the reciprocal lattice with magnitude $1/d_H$ where d_H is the interplanar spacing for the (H) set of

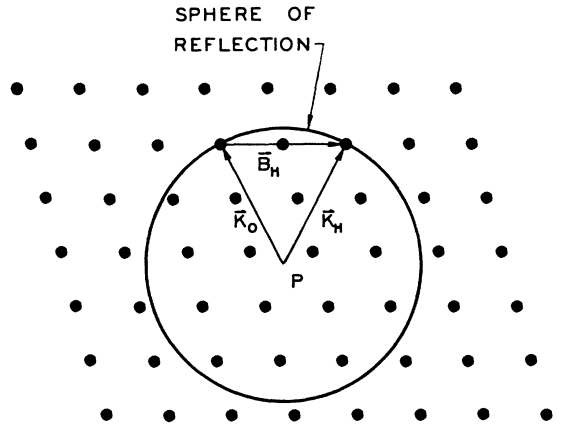

FIG. 2. Ewald's construction of the Bragg relation. The vectors connecting the lattice points of this figure constitute the family of reciprocal lattice vectors one of which $\mathbf{B}_H$ is shown. $\mathbf{K}_0$ and $\mathbf{K}_H$ are the propagation vectors for the incident and scattered radiations, respectively. Only those lattice points lying on or very near the propagation sphere will define the allowable propagation vectors.

planes. We shall only be concerned with the case where two propagation vectors are present.

In passage through the crystal the primary beam will suffer extinction until the diffracted beam contains most of the energy. Then, the roles of diffracted beam and incident beam become reversed. Actually, (see Fig. 3) there is a periodic exchange of energy between the two allowed beams; the periodicity in space will be closely related to the distance in the crystal medium which corresponds to an attenuation of the primary beam of the order of $1/e$. This attenuation will be here assumed to take place entirely by diffraction, absorption being neglected. The dynamical theory gives for this

‡ It can be shown that for the symmetrical Laue case when the incident and diffracted beams make equal angles with the crystal plate Eq. (1) for the determination of the center of the diffraction maximum is exact. λ is in this case the wave-length in vacuum, hence there is no correction for refractive index.

extinction distance the following result[8] under the assumption that for Laue

$$t_x=[2r_0(|F_H|/V)Kd_H\tan\theta_B]^{-1}, \quad (2)$$

reflection the two propagation directions make equal angles with the face of the crystalline slab. K is the polarization factor, F_H the crystal structure factor,¶ V the volume of the unit cell and r_0 equals $e^2/(mc^2)$. The distance t_x is measured normal to the face of the slab. See Fig. 3. If it is measured instead in terms of the number of atomic reflecting planes effective for extinction, then

$$N_H=t_x\tan\theta_B/d_H \quad (3)$$

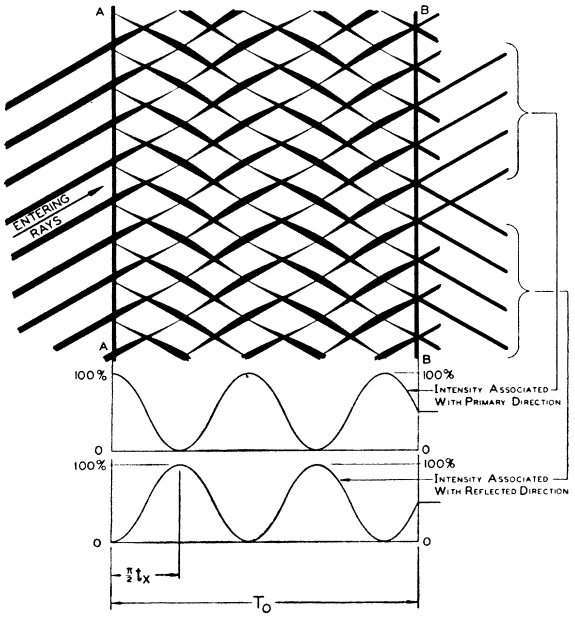

FIG. 3. The intensities of the two propagated beams are shown by the relative breadths of the corresponding rays. A periodic exchange of the energy from the one to the other beam takes place in the crystal. The distance which corresponds to a complete exchange of the energy from one beam to the other is $\pi/2t_x$. t_x is the extinction distance. Because of the surface irregularities, the two beams emerging will on the average each contain one-half the energy. For this reason, the emerging rays are shown with a breadth one-half the maximum.

[8] See reference 7, pp. 123–135.

¶ It might at first be thought that for the very short nuclear gamma-ray wave-lengths whose reflection coefficients are here measured, the coherent scattering would be completely negligible, and since only the coherent part of the scattered radiation can contribute to the selective diffraction by the crystal, one would be tempeted to expect no selective reflection whatever. The Compton shifted scattering is incoherent and plays no role in selective diffraction.

In order that coherent scattering shall occur, the final state of the atom after scattering must be the same as its initial state. The probability that an atom will scatter a photon and return to its initial state (coherent scattering) is a function only *of the change in momentum of the radiation* before and after scattering. So long as the scattering takes place at the Bragg angle, the change in momentum is constant independent of the wave-length. In calculating the structure factor F_H no account therefore need be taken of any variation with wave-length in the probability of coherent scattering. See A. H. Compton and S. K. Allison, *X-Rays in Theory and Experiment* (D. Van Nostrand Company, Inc., New York, 1935), pp. 252–253.

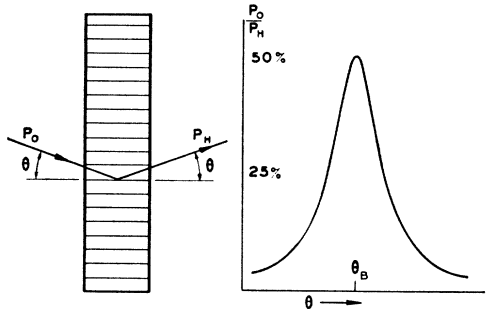

FIG. 4. This figure illustrates an idealized experiment to determine the reflection power of a crystal. P_0 and P_H represent the intensities, respectively, in the incident and diffracted beams. It is assumed that the radiation is *strictly* monochromatic and that the incident beam is a plane-parallel wave. The curve represents the fraction of the power which is diffracted as a function of the angle of incidence in the neighborhood of the Bragg angle θ_B. The equality of angles of incidence and diffraction is true only when the angle of incidence is θ_B in this Laue case.

so

$$N_H=[2r_0K(|F_H|/V)d_H^2]^{-1}. \quad (4)$$

This is a good measure of the maximum number of planes which can at any setting contribute coherently to the scattered amplitude. It is well known that the resolving power $d\lambda/\lambda$ of a grating in the first order is proportional to $1/N$ where N is the total number of lines in the grating. In the case of a crystal grating, this relation is

$$d\lambda/\lambda=1/(\pi N_H). \quad (5)$$

From the Bragg relation, we have $d\lambda/\lambda=d\theta/\tan\theta_B$ so $d\theta=\tan\theta_B/(\pi N_H)$. Set the width w of the diffraction pattern at half-maximum in radians equal to $d\theta$, then

$$w=2r_0K(|F_H|/V)d_H^2\tan\theta/\pi, \quad (6)$$

$$w=r_0Kd_H(|F_H|/V)\lambda/(\pi\cos\theta_B). \quad (6.1)$$

This is the same result which follows from the rigorous theory.

To define the "diffraction pattern," we must describe a somewhat idealized but not conceptually impossible experiment. Referring to Fig. 4, we think of a beam of extremely monochromatic and extremely parallel x-rays falling on a set of crystal planes at glancing angle θ. We then vary θ over a region of values in the neighborhood of the Bragg angle and we plot *the ratio of the power in the diffracted beam to the power in the incident beam* as a function of θ. The resulting curve exhibiting a maximum at say θ_B and falling rapidly on either side to very low values is called the "diffraction pattern." The words "extremely monochromatic" and "extremely parallel" used are to be interpreted as meaning that these qualities are pushed sufficiently far so that the effect of any residual inhomogeneity on the shape of the observed diffraction pattern becomes negligible. The diffraction pattern can be roughly characterized by giving its width at half-maximum height and the maximum value of the reflection coefficient at the peak of the

TABLE I. Summary of results for the four cases of special interest.

Type		Integrated reflection coefficient (Laue case)	Half-width of diffraction pattern at half-maximum
Perfect	Thick	$\frac{r_0 d_H K(\lvert F_H\rvert/V)\lambda}{2\cos\theta_B}$	$\frac{r_0 d_H K(\lvert F_H\rvert/V)\lambda}{\pi\cos\theta_B}$
	Thin	$\frac{r_0^2 d_H K^2(\lvert F_H\rvert/V)^2\lambda^2 T_0}{(\cos\theta_B)^2}$	$\left(\frac{\ln 2}{\pi}\right)^{\frac{1}{2}}\frac{d_H}{T_0}$
Mosaic	Low primary and secondary extinction	$\frac{r_0^2 d_H K^2(\lvert F_H\rvert/V)^2\lambda^2 T_0}{(\cos\theta_B)^2}$	$(\ln 4)^{\frac{1}{2}}$
	Primary extinction present. Low secondary extinction	$\frac{r_0 K(\lvert F_H\rvert/V)\lambda T_0 d_H}{2\cos\theta_B t_0}$	$\eta(\ln 4)^{\frac{1}{2}}$

pattern. Another very important quantity derived from the diffraction pattern is the *total area under the curve*. This we shall call the integrated reflection coefficient. Since the ordinates of the diffraction pattern are pure numbers (reflection coefficients) and the abscissas are angles, it follows that the integrated reflection coefficient is an angle. It is generally and will here be expressed in radians. It is in fact the equivalent angular range over which at 100 percent efficiency the same total amount of reflection would occur. The diffraction pattern widths of many crystals of perfect type are so small (of the order of a second of arc or less) that in practice x-ray beams are seldom defined in direction (at least by means of slits) with comparable homogeneity. The integrated reflection coefficient therefore is a very important factor in determining the power which will be associated with an x-ray reflection since it essentially determines the usable solid angle into which an emitting atom in an x-ray source can shine in order to be selectively reflected by the crystal planes.

If P_0 and P_H are intensities in the incident and diffracted plane parallel beams, respectively, then the integrated reflection coefficient is defined by

$$R_\theta=\int_{-\infty}^{\infty}[P_H(\theta-\theta_B)/P_0]d\theta. \tag{7}$$

Ewald's theory shows that for symmetrical Laue reflection in an ideally perfect crystal lattice, the shape of the diffraction pattern is that of a "witch" or resonance curve if the slab is sufficiently thick to include a large number of the intensity oscillations illustrated in Fig. 3. Since the distance t_x corresponding to the "wavelength" of one such oscillation is in most cases extremely small in comparison to the thickness of the slab, T_0, the assumption usually made is that the diffracted beam in different parts of the exit surface emerges *in all different phases* of the intensity oscillation. Therefore, for the case of a thick slab, the observed intensity is taken (by averaging uniformly over all phases) to be *half* the value occurring at the maximum intensity of the oscillations. These considerations show that for a thick crystal the maximum of the diffraction pattern will be a constant, $\frac{1}{2}$, independent of λ. For this case, only the width w will therefore depend on λ. The integrated reflection coefficient for the Laue case is:

$$R_\theta=\tfrac{1}{2}\pi w=r_0 K d_H(\lvert F_H\rvert/V)\lambda/2\cos\theta. \tag{7.1}$$

This is the value given in Table I.

The distinction between "thick" and "thin" crystals can only be made in terms of the extintion distance t_x. A thin crystal is one whose thickness T_0 is much less than t_x. In this case, the number of scattering planes is given by

$$N_H=T_0\tan\theta/d_H. \tag{8}$$

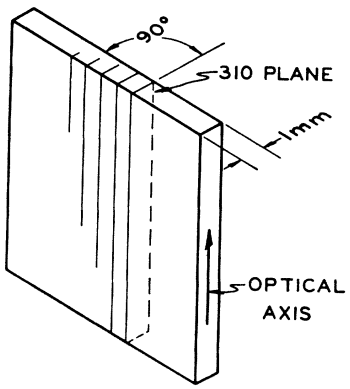

FIG. 5. The (310) lattice planes of quartz lie so that they are parallel to the edge of the crystal wafer and normal to the major faces of the wafer. The crystal was bent elastically so that the "c" or optic axis, and therefore the (310) planes, lay parallel to the generators of a right circular cylinder.

Again $d\lambda/\lambda$ is proportional to $1/N_H$ so

$$d\lambda/\lambda=kd_H/(T_0\tan\theta),$$

where k is a proportionality constant of order one-half, from which it follows that the width of the diffraction pattern w is given by

$$w=kd_H/T_0. \tag{9}$$

The theory predicts $k=(\pi^{-1}\ln 2)^{\frac{1}{2}}$. The angular width of the diffraction pattern is now independent of the wave-length. The intensity diffracted by the crystal is proportional to the square of the diffracted amplitude. The amplitude will be given by

$$r_0 K(\lvert F_H\rvert/V)\lambda T_0/\cos\theta_B.$$

The integrated reflection coefficient will then be proportional to the square of the amplitude and to the diffraction pattern width. That is,

$$R_\theta\propto[r_0 K(\lvert F_H\rvert/V)\lambda T_0/\cos\theta_B]^2 d_H/T_0.$$

The dynamical theory predicts the integrated reflection

coefficient to be

$$R_\theta = r_0^2 d_H K^2(|F_H|/V)^2\lambda^2 T_0/\cos^2\theta_B. \quad (10)$$

Thus, our simple considerations lead to the same result as the more rigorous theory. The conditions in a mosaic crystal can be understood in terms of these two results (7.1) and (10) for a perfect crystal. If the mosaic units are perfect and of such size that the primary extinction is small, then each unit will scatter an intensity proportional to

$$[r_0 K(|F_H|/V)\lambda t_0/\cos\theta_B]^2,$$

where t_0 is an appropriate mosaic unit dimension. The integrated reflected intensity per mosaic unit will be

$$R_\theta' = r_0^2 K^2(|F_H|/V)^2\lambda^2 d_H t_0/\cos^2\theta. \quad (11)$$

Now the further assumption is made that in every layer of crystal dx there exists a distribution function for the orientation of these individual units in that layer. The number of mosaic units in the layer dx will be proportional to dx/t_0. The angular orientations of the blocks are assumed to be distributed about a mean orientation as given by

$$w(\Delta) = (2\pi\eta)^{-\frac{1}{2}} \exp(-\Delta^2/2\eta^2), \quad (12)$$

where Δ is the deviation from the mean and η is the distribution parameter. Hence, the total integrated reflected intensity from the layer dx will be given by

$$r_0^2 K^2(|F_H|/V)^2\lambda^2 d_H dx/\cos^2\theta_B, \quad (13)$$

provided we explore a sufficient angular breadth to accommodate all the orientations covered under (12). Thus, the intensity reflected by the crystal will be

$$R_\theta = r_0^2 K^2(|F_H|/V)^2\lambda^2 d_H T_0/\cos^2\theta_B. \quad (14)$$

The width of the diffraction pattern will be given by $\eta(\ln 4)^{\frac{1}{2}}$ provided the diffraction width for the individual units, $(\pi^{-1}\ln 2)^{\frac{1}{2}} d_H/t_0$ is less than $\eta(\ln 4)^{\frac{1}{2}}$. The integrated reflection coefficient as written assumes that secondary attenuation, as well, is negligible. The expression for the case of large primary extinction but small secondary attenuation follows by similar arguments. Since the primary extinction is large, one may substitute the expression (7.1) for Eq. (11) in the development just preceding.

The results for the four cases of special interest are tabulated in Table I. It is recognized that the interpretation of the experimental results for the curved crystal by the formulas derived for an unstressed crystal may not be valid but the comparison will be useful toward understanding the phenomena.

The method of the curved-crystal spectrometer described in this paper *permits only measurements of R_θ, the integrated reflection coefficient*, but unfortunately *does not afford any means with our present facilities of estimating t_0 the size of the domains* in the crystal over which coherent reflection can take place. Reference to formula (14) shows that R_θ is independent of t_0. A study of the structure of the undoubtedly very narrow intrinsic diffraction pattern of the quartz lattice is at present beyond the reach of even the very high resolving power attained in our two-meter curved-crystal instrument. We have in fact no clear-cut experimental evidence that any mosaic structure exists at all in elastically bent quartz save that to date this assumption is the only one we have found to explain the observed fact that for such quartz R_θ is proportional to λ^2 over the wide range of wave-lengths we have covered. Unstressed quartz, on the other hand, for which R_θ is more nearly proportional to λ, turns out to behave more nearly like an ideally perfect lattice over the limited range of wavelengths with which we have been able to study it by the two-crystal spectrometer method. Our reason therefore for presenting here brief accounts of the results of the dynamical theories of x-ray reflection for both ideally perfect and mosaic crystals is merely to permit a comparison of these with our observed results. We make no claim that any such theories satisfactorily fit the observed facts.

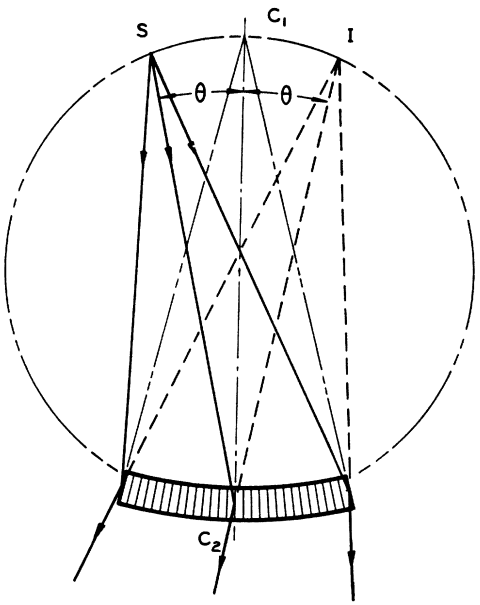

FIG. 6. The fundamental geometry of the curved-crystal focusing spectrometer used in transmission is shown. The crystal lamina is bent to a radius equal to the diameter of the focal circle. S represents the source position, C, the intersection of the atomic planes on the focal circle, and I the virtual source of the radiation after diffraction by the lattice. The neutral axis of the bent crystal is tangent to the focal circle at C_2. This geometry is not exact because the neutral axis should coincide with the focal circle over the whole crystal.

EXPERIMENTAL TECHNIQUE

Entirely different experimental methods were used for measuring the integrated reflection coefficients for the stressed and unstressed quartz plates. The quartz crystals used in this investigation were cut so that the (310) planes lay parallel to one edge and normal to the plane of the plate (Fig. 5). These are the same crystals which are used in the gamma-ray spectrometer de-

scribed by DuMond.[1] The plates were polished to an optically flat finish on the major faces. When used in the curved-crystal spectrometer, the crystal plate is bent elastically so that it has with extremely high accuracy the shape of a right circular cylinder with a radius of approximately two meters. This bending is accomplished by clamping the crystal between two blocks of stainless steel provided with holes for the passage of the radiation.

The vise-like jaws so formed are cylindrically profiled, one convex, the other concave, with a radius of curvature of two-meters. Only the convex surface is profiled to high precision, the crystal being held in intimate contact with it by means of a rubber cushion placed between the crystal and the concave vise jaw.

Figure 6 shows the essential geometry of the focusing curved-crystal spectrometer. The crystal shown at C_2 is elastically deformed so that the crystal planes intersect at the point C_1. Since the point S lies on the circle through C_1 and C_2 having C_1C_2 as a diameter, all rays leaving S and striking the crystal will make the same angle with the atomic planes. In order to have exact focusing, it is necessary that the crystal lamina lie on the focal circle. This condition is not exactly satisfied in the present spectrometer but the aberrations introduced by failure to meet the condition are entirely negligible. The diffracted rays will appear to come from the virtual source I. It is readily seen that this arrangement affords a tremendous gain in luminosity over the usual flat-crystal spectrometer. The aperture angle available to the source is just the angle which the crystal subtends at the source.

Figure 7 shows schematically just enough of the essential elements of the instrument to clarify the method of measuring reflection coefficients with it. In the gamma-ray case, the source at S consists of a thin strip of neutron-activated material while in the x-ray case a thin metal strip at the same point is exposed (from the side) to primary x-radiation which causes it to emit its characteristic fluorescent x-radiation. This radiation emerges from the radiator surface at a small grazing angle and passes to the curved crystal at C_2. Here the radiation, diffracted at the Bragg angle θ on the crystal planes, is deviated through an angle 2θ and emerges as a divergent beam with the image point I as its virtual source. It then passes through the diverging collimator whose function is to arrest the strong direct radiation from S transmitted without deviation through the crystal. By mechanical means not here shown, both S and C_2 are moved so as to explore the spectrum but maintain the diffracted beam always strictly aligned with the collimator. The intensity of the diffracted beam is then measured in a special "multicellular" Geiger counter.[9] As S approaches I a point P determined by the collimator geometry will be reached at which the directly transmitted beam will start to leak through the collimator channels to the counter. Beyond this point, the spectrometer cannot be used as such. However, by setting the source S exactly at I, a good measure of the intensity of the entire direct undiffracted beam can be made and this is very useful in the determination of reflection coefficients. Such a direct measurement is so many thousands of times stronger than the reflected beam that it is necessary to attenuate the direct beam with a series of absorbing plates or foils. The true unabsorbed intensity of the line radiation in question can then be obtained by extrapolating on a semilogarithmic absorption plot back to the counting rate for zero absorber.

It would be a mistake, however, to suppose that the ratio of direct to diffracted intensities observed in the way roughly indicated can be taken directly as the

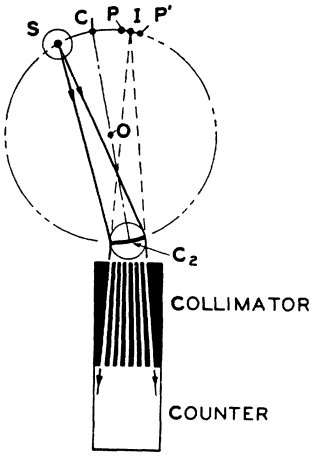

FIG. 7. The essential elements of the curved-crystal focusing spectrometer as used for the study of the reflection properties of the (310) planes of quartz. The source is placed on the focal circle at S, and the radiation diffracted by the crystal appears to come from the point I. The collimator only serves to prevent the directly transmitted beam from detection by the counter placed behind the collimator. PP' is the arc inside of which the source S can radiate directly through the collimator into the counter.

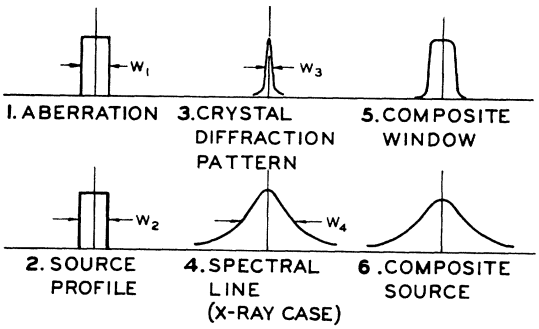

FIG. 8. This figure shows the form of the four profiles which determine the nature of the experimentally observed line profile in the curved-crystal spectrometer, (1) the assumed focal aberration of the curved crystal, (2) the finite source size, (3) the intrinsic diffraction pattern of the crystal, and (4) the spectral distribution of the x-ray or gamma-ray line. The composite window 5, (fold of 1 and 3) may be considered the tool which is used to explore the composite source 6, fold of (2 and 4).

[9] D. A. Lind, Rev. Sci. Inst. **20**, 233 (1949).

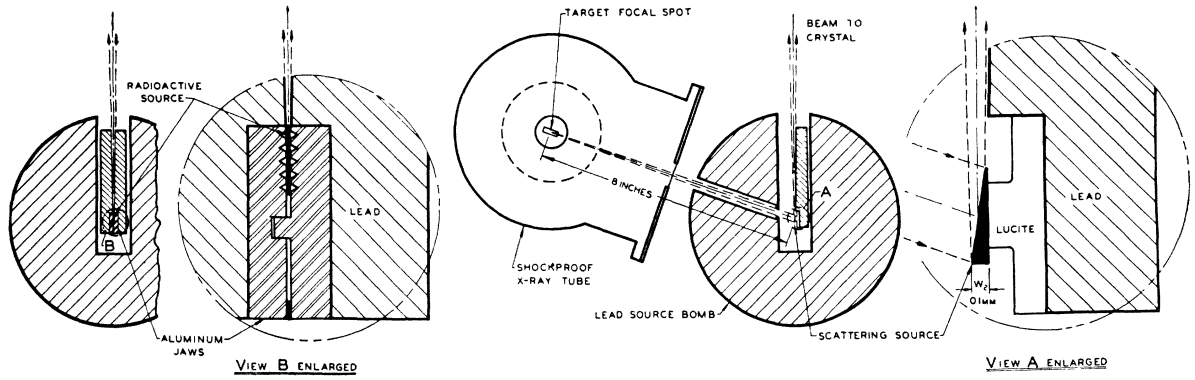

FIG. 9. Source geometry for x-ray and nuclear gamma-radiation sources. The x-ray source is a piece of metal foil ground to the shape of a thin wedge and placed at the center of the lead source bomb. This foil is irradiated with the continuous radiation from a tungsten target x-ray tube at the left. The nuclear gamma-sources are metal foils activated by neutron bombardment. These foils are clamped between the aluminum jaws of the holder to define the source geometry accurately. The surrounding lead defines the angular divergence of the beam so that it will just fill the crystal aperture. This source assembly is mounted in the lead source bomb in place of the x-ray scattering source holder.

reflection coefficient. A number of instrumental factors in addition to the reflection properties of the crystal determine this observed ratio as follows:

(1) The bending of the crystal in the profiled vise never succeeds in focusing the atomic planes with absolute perfection at C_1. Instead a small aberration pattern of finite width w_1 in the focal circle is formed. (2) The source is not an infinitesimal line but has also a finite width w_2 on the focal circle. Furthermore, (3) the intrinsic diffraction pattern of the crystal, as we have already pointed out, has an angular width w which may be translated into linear measure w_3 on the focal circle, and finally (4) the spectral line under study has a natural spectral width $\delta\lambda$ which may also be translated into linear units giving a width w_4 on the focal circle. Figure 8 gives an idea of the shapes of these different patterns. The "shape" of an observed spectral line is then explored with the spectrometer by plotting the counting rate for successive closely spaced positions of the source S on the focal circle relative to the crystal C. Actually, this process can be thought of as a superposition of all four of the above patterns. Patterns (1) and (3) associated with the crystal can be thought of as folded together to form a composite exploring "tool" or "window" (pattern 5 in Fig. 8) while patterns (2) and (4) are folded together to form a composite source profile (pattern 6 in Fig. 8). As this tool explores across the source profile, the maximum intensity will be observed when the product integral of the two composite profiles has its maximum value, i.e., at the point where all four separate profiles overlap most advantageously. Clearly then, the modus of this overlapping is of great importance in determining the observed intensity whereas R_θ the integrated reflection coefficient which we seek to measure depends on only one of the four patterns.

By an analysis of the four pattern shapes, one of us[10] has derived formulas which permit the calculation of R_θ the integrated reflection coefficient of the crystal from a quantity Γ_λ which is easy to obtain from the direct observations and which has the following definition. Γ_λ is the ratio of two quantities, in the numerator, (1) the peak line intensity (counting rate), $R_A(0)$, observed in the diffracted beam as the spectrometer explores across a given spectral line of wave-length λ with the source in position S (Fig. 7) and (2) in the denominator that fraction, γ_λ, of the peak primary intensity (counting rate), R_D, which is associated with the same line λ and which is observed in the divergent direct beam transmitted through the crystal with the source in position I (Fig. 7). The spectral composition of the entire measured radiation in the direct neam must, of course, be known in order to determine the fraction γ_λ associated with the line λ. The formula for Γ_λ as defined above is then

$$\Gamma_\lambda = R_A(0)/(\gamma_\lambda R_D). \tag{15}$$

In order to compute R_θ from Γ_λ, the following reasonable assumptions were made regarding the four profiles of Fig. 8. (1) The linear extension w_1 of the focal aberration pattern and the width w_2 of the source on the focal circle are approximately equal and they are large compared to the width w_3 of the intrinsic crystal diffraction pattern. The focal aberration pattern was carefully studied by observing with the spectrometer the exact positions of the centers of line-profiles formed by utilizing different portions of the curved crystal (isolated with a stop), a method analogous to the Hartmann test in optics. This aberration pattern had a width** $w_1 = 0.1$ mm on the focal circle. The widths, w_2, of the sources were purposely made as nearly as possible

[10] D. A. Lind, thesis, California Institute of Technology (1948).

** By improvements in the crystal clamp profiling, we have subsequently succeeded in reducing w_1 to 0.05 mm.

TABLE II. Table of data and derived results from R_θ.

Line	λ x.u.	E Mev	Γ_i[a]	Γ_i/R_θ from theory	R_θ x.u.[b]	R_θ radians
Sn $K\alpha_1$	489.57	0.0253	0.175±0.023	2.27	7.70×10^{-2}	$(3.28\pm0.43)\times10^{-5}$
Ta $K\alpha_1$	214.88	0.0506	0.050±0.002	3.20	1.56×10^{-2}	$(6.63\pm0.27)\times10^{-6}$
Au $K\alpha_1$	179.96	0.0688	0.044±0.004	3.39	1.30×10^{-2}	$(5.52\pm0.50)\times10^{-6}$
Th $K\alpha_1$	132.3	0.0936	0.017±0.004	3.62	4.69×10^{-3}	$(1.99\pm0.47)\times10^{-6}$
Au^{198}	30.09	0.411	0.0030±0.0001	8.33	3.60×10^{-4}	$(1.53\pm0.05)\times10^{-7}$
Co^{60}	10.578	1.172	$(4.97\pm0.50)\times10^{-4}$	8.33	5.97×10^{-5}	$(2.54\pm0.25)\times10^{-8}$
	9.308	1.332	$(4.12\pm0.50)\times10^{-4}$	8.33	4.95×10^{-5}	$(2.11\pm0.25)\times10^{-8}$

[a] Γ_i is the ratio of the peak counting rate at the line to the counting rate in the incident beam, and hence, represents the fraction of incident quanta which is selectively diffracted at the maximum of the line profile. Γ_i is not a constant of the crystal but depends on instrumental factors as well.
[b] In this column the angle R_θ which is usually expressed in radians is instead expressed in x units.

equal to the aberration width w_1. (2) The wave-length distribution (spectral line profile) of the line of wave-length λ under observation must be assumed to be known. In the x-ray cases, the spectral profiles can safely be assumed to be "witches" and the widths can be found from previous two-crystal spectrometer data. In the gamma-ray cases, there are good reasons for believing that the spectral line widths w_4 used in these observations are far too narrow for detection, a condition which simplifies the calculations of R_θ from Γ_λ. For brevity, most of these calculations and the derivations of the formulas on which they are based are here omitted. As an example, however, take the gamma-ray case of a line of negligible spectral width w_4.

If one focuses attention on an infinitesimal areal element of the crystal and asks what fraction of the source will radiate quanta which will pass through this element so as to make angles of incidence with the (310) planes lying within the crystal diffraction pattern, one will see that this fraction is proportional to $R_\theta D_f/t$, where R_θ is the integrated reflection coefficient, D_f the focal circle diameter and $t=w_1=w_4$ is the linear extension of the source (and also the focal aberration) at the focal circle. This follows because $R_\theta D_f$ is the width on the focal circle of that part of the source from which radiation can be selectively diffracted by any given element of crystal. This is just the result which is derived from a more general and exact analysis. By a similar analysis any case can be reduced to give an expression for Γ_λ in terms of R_θ provided the above-stated assumptions are fulfilled.

To make a reliable determination of Γ_λ, a source of known spectral composition is needed so that γ_λ shall be known. In the x-ray region, the fluorescent K radiation from an element of high atomic number is satisfactory since the continuous background from Compton scattering can be kept very small. Figure 9 shows a schematic drawing of the source arrangement. The x-ray tube excites in the scatterer its characteristic fluorescent radiation as well as Compton-scattered radiation. However, very little of the Compton scattering is directed toward the crystal because the scattering angle is about 110° and the atomic number is high. Nevertheless, to eliminate all question as to the effect of continuous scattered background, a procedure utilizing the Ross method of "balanced filters"[11] was employed. By this procedure, the direct beam was observed with a pair of filters which were designed so that their K edges bracketed the line under study. The *difference* between these readings then represented the sum of the fluorescent radiation *plus only the Compton scattering which lay in the small wave-length interval bracketed by the filters*. At the same time, the peak reading at the line was also made with the same transmission filters.

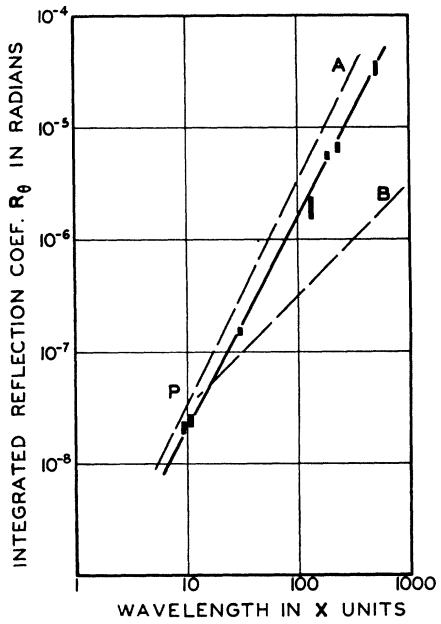

FIG. 10. Reflection properties of elastically curved-quartz plate. The full line is a plot of the measured integrated reflection coefficient R_θ for the (310) planes of quartz in the Laue or transmission case as a function of the wave-length λ. The ordinate scale is in radians and the abscissa scale is in x.u. The experimental points are shown with their probable errors (vertical heights of the rectangles). (The probable error of the wave-length is completely negligible on this plot.) Curve A represents the theoretical behavior of a similar quartz plate if the crystal behaved as a mosaic with small primary and secondary extinction. The curve B represents its behavior if it were perfect. In the region of the intersection P of the curves A and B, the primary extinction distance is of the same order as the plate thickness. Below this point, curve B should coincide with curve A.

[11] P. A. Ross, J. Opt. Soc. Am. and Rev. Sci. Inst. **16**, 433 (1928); P. Kirkpatrick, Rev. Sci. Inst. **10**, 186 (1939).

The actual source mounted in the spectrometer was the scattering foil. See Fig. 9. This was prepared of pure metal foil 0.004 in. thick by grinding to the shape of a thin wedge. Foils of Sn, Ta, Au, and Th were used. Great care was taken to make the sources identical in projected geometrical width w_2 as seen by the curved crystal. This required mounting them so that their projected width on the focal circle was 0.1 mm and no more. The width of 0.1 mm represented also the linear extent of the focal aberration of the curved crystal at the focal circle. The foils were mounted on a Lucite support by means of stopcock grease which was sufficiently tacky to hold them, yet did not dry and distort their shape. The x-ray tube was mounted so that the target-source distance remained always at 8 in. Preliminary calculations had shown that a tungsten tube operating at 150 kvp and 10 ma would generate sufficient fluorescent radiation for these measurements, thanks to the high luminosity of the curved-crystal instrument with the source at the focus.

The peak intensity in the diffracted $K\alpha_1$ line from each source and the intensity of the incident beam were measured with the Ross filters. In the case of thorium $K\alpha_1$, no filter was available but an extrapolation of the corrections to the measurements at gold showed this correction for Compton-scattered continuous radiation to be negligible. The relative intensities of the lines of the K spectra have been measured.[12] From these data it is possible to determine the factor γ_λ in Eq. (15).

In the determination of the values of Γ_λ for the nuclear gamma-radiations[13,14] from Au^{198} and Co^{60}, the only difference from the x-ray measurements was that in each case the source was a piece of a pure activated metal foil mounted as shown at B in Fig. 9. The foil was 5 mm wide by 30 mm long by 0.1 mm thick and was activated by neutron bombardment at Oak Ridge. It was necessary in these cases to know the decay scheme so that the values of γ_λ could be evaluated. In gold, only the 0.41-Mev gamma-line was assumed to be present while in cobalt it was assumed that the 1.17- and 1.33-Mev lines were in cascade.†† In every case the data were corrected for background counting rate.

In the gamma-ray cases, lead defining jaws were used to limit the angular dimensions of the beam transmitted from the source to the crystal. The width w_2 of the source on the focal circle was however determined by the thickness of the source foil itself.

The experimental determinations of Γ_λ were reduced to R_θ by the expressions relating Γ_λ and R_θ which are found by Lind.[10] They take slightly different forms for the x-ray and gamma-ray lines because the inherent spectral line widths are different for the two cases. The spectral line widths for the $K\alpha_1$ lines of tungsten and silver were taken from Compton and Allison.[15] By linear interpolation, the values for the other elements were obtained. The line widths for the nuclear gamma-lines were assumed to be very much smaller than any other factors contributing to the diffracted line profile; hence, it was not necessary to know these values. Table II contains the data which were obtained, together with the derived results for R_θ.

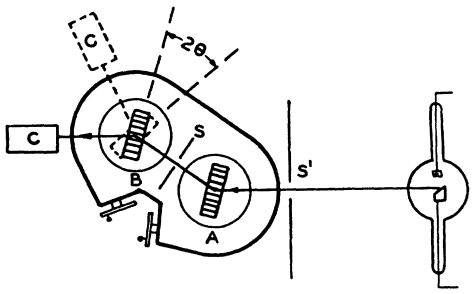

FIG. 11. Schematic illustration of the two-crystal x-ray spectrometer employing the (310) planes (transmission or Laue case) of two identical quartz plates, 1 mm thick. The full lines show the general position for the parallel rocking curve. The dotted lines show the position for the antiparallel rocking curve. The slits or stops are at S and S'. The xenon-filled counter is at C.

INTERPRETATION OF THE EXPERIMENTAL RESULTS

Table II shows the experimental results on the measurement of Γ_i and their reduction to R_θ. In Fig. 10 is shown the plot of the resulting data. The slope of the curve of R_θ *versus* λ on a logarithmic plot is slightly less than two. However, the discrepancy when compared with the curve of slope 2 is not outside deviations which might be accounted for by experimental errors. The probable errors which are shown *represent only the statistical errors in the observed data.* It must be pointed out that there are a number of other factors which could influence the exact value of R_θ. The presence of scattering from certain parts of the instrument when the intensity of the direct beam was measured would have the effect of depressing the curve more at short wave-lengths than at long wave-lengths. The assumptions involved in the reduction of the experimental value Γ_λ to R_θ introduce, perhaps, the largest uncertainties. It is believed that the additional uncertainty introduced by all such factors would probably not exceed plus or minus 25 percent. On the logarithmic scales shown, this would not greatly modify the data.

A calculation of the theoretical value of R_θ for the (310) planes of quartz is made as follows. From Table I the value of R_θ for a mosaic-like crystal is

$$R_\theta = r_0^2(|F_H|/V)^2K^2\lambda^2 d_H T_0/(\cos\theta_B)^2. \qquad (14)$$

Because the radiation is unpolarized, the value $\langle K^2\rangle_{Av}=\frac{1}{2}(1+\cos^2 2\theta_B)$ is substituted for K^2.

[12] Compton and Allison, see reference ¶, pp. 638–641.
[13] DuMond, Lind, and Watson, Phys. Rev. **73**, 1392 (1948).
[14] Lind, Brown, and DuMond, Phys. Rev. **76**, 1838 (1949).
†† Direct measurements on Co^{60} with this instrument have confirmed the equality of intensity of the two lines.

[15] Compton and Allison, see reference ¶, pp. 745–746.

TABLE III. Observations on the transmission diffraction patterns from the (310) planes of quartz. The factor $\exp[\mu_0 t_0/\gamma_0]$ corrects the specified data for the absorption of the beam in the crystal plate since the crystals are used in transmission throughout.

(A)	$R\exp[\mu_0 t_0/\gamma_0]\times10^6$ (radians) Obs. (310)	Obs. $(\bar{3}\bar{1}0)$	Calc. (310) or $(\bar{3}\bar{1}0)$	$P(0)\exp[\mu_0 t_0/\gamma_0]$ Obs. (310)	Obs. $(\bar{3}\bar{1}0)$	Calc. (310) or $(\bar{3}\bar{1}0)$	W_θ (seconds of arc) Obs. (310)	Obs. $(\bar{3}\bar{1}0)$	Calc. (310) or $(\bar{3}\bar{1}0)$
0.710±0.0020[a]	2.58	2.77	2.30	0.172	0.161	0.246	1.1	1.3	0.53
0.530±0.0074[a]	2.02	2.12	1.65	0.134	0.136	0.250	1.2	1.2	0.42
0.320±0.0076[a]	1.50	1.51	1.00	0.116	0.111	0.250	1.1	1.0	0.26
0.210±0.002[b]	1.30	1.63	0.657	0.123	0.128	0.250	0.73	0.92	0.17
0.123±0.0084[b]	0.89	1.04	0.389	0.115	0.890	0.250	0.54	0.88	0.10

[a] Molybdenum tube used for the x-ray source.
[b] Tungsten tube used for the x-ray source.

The maximum value of θ_B is about 12° so, one may set $\langle K^2\rangle_{Av}/\cos^2\theta_B=1$ with an error of 10 percent or less. Hence,

$$R_\theta \cong r_0^2(|F_H|/V)^2\lambda^2 d_H T_0.$$

Substituting the following data:

$$T_0=1\text{ mm},\quad d_{310}=1.178\text{A},\quad |F_{310}|=21.0,$$
$$V=112\text{A}^3,\quad r_0=2.82\times10^{-5}\text{A},$$

hence, we obtain the result

$$R_\theta=3.29\times10^{-4}\lambda^2.$$

R_θ is in radians and λ in A. This result is graphically plotted as curve A in Fig. 10 for comparison with the experimental results. The corresponding formula for a perfect thick crystal is

$$R_\theta=r_0(|F_H|/V)K\lambda d_H/(2\cos\theta_B). \qquad (7.1)$$

Again set

$$\langle K\rangle_{Av}/\cos\theta_B=1,$$

we obtain for the result

$$R_\theta\cong3.14\times10^{-6}\lambda.$$

This is plotted as curve B in Fig. 10.

It should be noted that for the range of λ for which $T_0<t_x$, i.e., for which the primary extinction distance is greater than the thickness of the plate, the "perfect" crystal behaves as would the "mosaic" as far as integrated reflection is concerned. It is interesting to note that for every thickness of crystal, the mosaic crystal will have the *higher reflection coefficient* until the perfect crystal no longer may be considered thick. The numerical agreement of the observed results with the "mosaic model" (curve A, Fig. 10) is quite good considering the nature of these measurements. The mosaic-like behavior of the stressed- (curved-) quartz plates was a source of some surprise. There is no reason to think that bending the quartz plate introduces any *permanent* irreversible disorder in the structure since the crystalline quartz behaves perhaps more nearly perfectly elastically than any other known substance.

These results prompted one of us (W.J.W.) to carry out determinations of the integrated reflection coefficients and diffraction pattern widths over a part of the same range of wave-lengths for the (310) planes of identical *unstressed* quartz crystals.

MEASUREMENTS OF THE REFLECTION PROPERTIES OF UNSTRESSED-QUARTZ PLATES

The two-crystal spectrometer designed by DuMond[16] was used to measure the reflection properties of the (310) planes of unstressed quartz over a wave-length range from 0.123 to 0.707A. The great flexibility of this high precision instrument afforded by its four separate worm-wheel adjustments permitted the easy realization of many of the requisite conditions which would have been made much more difficult or impossible with other less flexible designs. The two-crystal method has been adequately described.[17] It is well known that the "parallel" position curves give information concerning the crystal properties independent of the spectral distribution of the radiation. Figure 11 shows the two-crystal arrangement. The usual procedure is to set the crystal A so that a wave-length λ is reflected through the slit S to the crystal B. The crystal B is rocked about the position of parallelism with crystal A and the intensity as detected by the counter C is plotted as a function of the angle. Since this arrangement allows all wave-lengths to be transmitted, the wave-length band which is used is controlled by the slit system at S^1 which limits the horizontal (and also the vertical) angular divergence of the beam incident on crystal A. It can be shown that the power received by the detector, as crystal B is rotated through small angles, is a function only of the properties of the crystals and not of the spectral distribution or the geometry of the slit system.

The quantities which one can obtain are the integrated reflection coefficient R_θ, the half-value width of the diffraction curve and the peak Laue reflection of the crystal planes. (Peak value of the diffraction pattern of Fig. 4.) If a plane-parallel beam of monochromatic radiation falls on the crystal, the ratio of the intensity in the diffracted beam to that in the incident beam will be the ordinate of the diffraction pattern of Fig. 4 or the reflection factor. It is the maximum ordinate of this function and its half-maximum width which one can

[16] J. W. M. DuMond and D. Marlow, Rev. Sci. Inst. 8, 112 (1937).
[17] See reference 7, pp. 147–155.

measure. It has been shown that it is impossible however to obtain the *shape* of the diffraction profile from the parallel position rocking curve. The two-crystal spectrometer results cannot be reduced so as to give exactly these quantities, unless it can be proved by some other means that the diffraction pattern sought *is symmetrically distributed about a central point.* The usual procedure is to observe the ratio of the total power reflected by the internal planes of crystal B to the power incident upon it. If this quantity is designated by $P(\beta)$, the *two-crystal integrated reflection coefficient is* defined by

$$R'=\int_{-\infty}^{\infty} P(\beta)d\beta. \tag{16}$$

where β is the angle by which the atomic planes of crystal B deviate from parallelism with those of A. Equation (16) is analogous to the definition for R_θ, the integrated reflection coefficient for a single crystal. It can be shown that

$$R'=\frac{[{}^pR_\theta]^2+[{}^nR_\theta]^2}{{}^pR_\theta+{}^nR_\theta} \tag{17}$$

in the case that the incident radiation may be considered unpolarized. The superscripts p and n refer to the orientation of the plane of polarization of the incident radiation, p refers to the electron vector parallel to the plane of scattering and n, normal to said plane. If other absorption processes are present as well as anomalous dispersion, then

$$\exp[\mu_0 t_0/\gamma_0]R'=\left[\frac{1+\cos^2 2\theta_B+2l_0^2(1+\cos^4 2\theta_B)}{1+\cos 2\theta_B+l_0^2(1+\cos^3 2\theta_B)}\right]. \tag{18}$$

The terms in l_0 occur because of anomalous dispersion and are important only at wave-lengths in excess of about 400 x.u. The term $\exp[\mu_0 t_0/\gamma_0]$ is an attenuation factor. μ_0 is the total absorption coefficient while t_0/γ_0 is the true path length in the crystal. γ_0 is the cosine of the angle of incidence measured with the normal to the crystal plate.

W_θ, the half-maximum width of the two-crystal rocking profile, is given by

$$W_\theta=2w_\theta. \tag{19}$$

w_θ is the half-maximum width of the single crystal Laue diffraction pattern.‡‡ Finally, the peak transmission $P(0)$ is given by

$$P(0)\exp[\mu_0 t_0/\gamma_0]=\frac{1}{4}\left[\frac{1+\cos 2\theta_B+(3/4)l_0^2(1+\cos^2 2\theta_B)}{1+\cos 2\theta_B+l_0^2(1+\cos^3 2\theta_B)}\right]. \tag{20}$$

It must be noted that if unpolarized radiation is used, it is impossible from the two-crystal rocking curves to

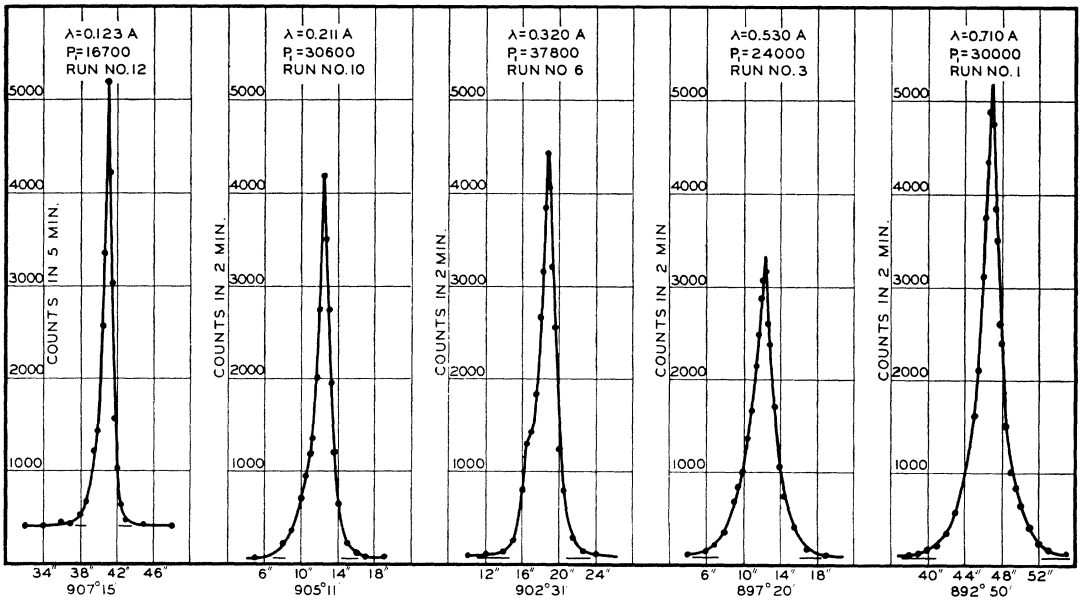

FIG. 12. Experimental Laue reflection rocking curves of the two-crystal x-ray spectrometer using the (310) planes of quartz in the first-order parallel position. P_i (given above each curve) is the number of counts in 2 min. for the "straight through" beam (off parallel setting) used for "normalizing" the curves. The angular positions indicated below each curve refer to the nominal setting of the spectrometer worm wheels. The points were taken at $\frac{1}{4}$ second intervals.

‡‡ The result Eq. (19) follows from the fact that the single-crystal Laue diffraction pattern for the symmetrical case has the profile of a witch or resonance curve. The half-maximum width of the fold of two witches is just the sum of the individual half-maximum widths.

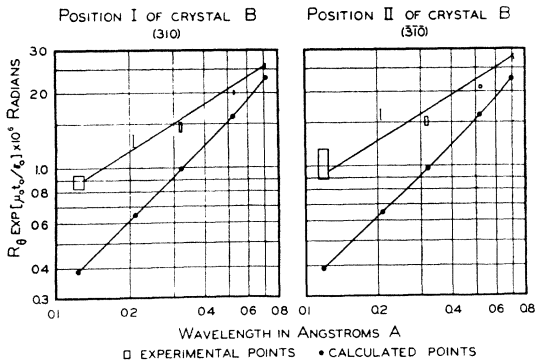

FIG. 13. Reflection properties of the (310) planes of the *unstressed*-quartz crystal. The log of integrated reflecting power is plotted *versus* the log of the wave-length to determine the dependence of the integrated reflecting power on the wave-length. These data were obtained on the two-crystal spectrometer. The widths of the rectangles, where these are used to locate the experimental points, give the ranges of wave-lengths transmitted by the spectrometer at each wave-length setting. The height of the rectangle gives the spread in the experimental intensity data. The position *II* of crystal *B* was obtained by rotating the crystal through 180° so that the (3$\bar{1}$0) planes were used.

calculate separately ${}^pR_\theta$ and ${}^nR_\theta$. The usual procedure is to make an assumption concerning the model and calculate the two-crystal quantities. $R'\exp[\mu_0 t_0/\gamma_0]$, $P(0)\exp[\mu_0 t_0/\gamma_0]$ and W_θ were calculated for perfect thick crystals to compare with the experimental data.

The x-ray source consisted of a molybdenum target tube driven by a full-wave rectified filtered supply, or a tungsten tube driven by a half-wave rectified supply. Manual control was used except in the filament circuit where a saturable core stabilizer was used.

The two quartz plates were carefully mounted so that both the (310) planes and the large flat faces of the slabs were accurately parallel¶¶ to the axes of rotation and so that the centers of the thickness of the plates were centered on these axes. Great care was taken to avoid introducing any stress in the quartz by the supporting means. The quartz plates were optically polished and parallel to several fringes, but the surfaces were not etched. Subsequent experience has shown that even with the most careful polishing technique, the surfaces should be etched to remove submicroscopic material wedged into the minute cracks. The wave-length band which the instrument accepts was adjusted by the setting of the jaws of the defining slit (placed midway between crystal pivots *A* and *B*, Fig. 11). It is, of course, easy to ascertain this setting by turning crystal *B* and the arm supporting the counter through the appropriate angles to permit study of the anti-parallel rocking curve which gives the spectrum of the radiation being used. The x-ray beam was 4 mm wide and 5 mm high at crystal *B*. The slits were always wide enough to permit the $K\alpha_1-\alpha_2$ doublet to pass. Certain curves were taken using a band of the continuous spectrum of approximately this same width.

The use of a xenon-filled thin window counter made it possible to use rather low intensity from the x-ray tube. The efficiency of the counter ranged from about one to 20 percent over the range of wave-lengths used. The counters, made with a cylindrical copper cathode, and a 7-mil tungsten wire anode, were filled to a pressure of 10 cm of Hg with a two to three percent mixture of petroleum ether in xenon.

The center of the wave-length band was selected by setting the crystal *A*. Crystal *B* was then set "off parallel" by a very small angle and the total radiation transmitted by the plate was measured. This datum was used to normalize the parallel rocking curve appropriately. The parallel position rocking curves were made first with crystal *B* as shown and then with *B* rotated through an angle of 180°. Since the reference datum is the beam transmitted "off parallel" by the crystal *B*, the absorption factor $\exp[-\mu_0 t_0/\gamma_0]$ is taken into account and one can compare $R'\exp[\mu_0 t_0/\gamma_0]$ and $P(0)\exp[\mu_0 t_0/\gamma_0]$ directly with the experimental data.

COMPARISON OF THEORETICAL AND EXPERIMENTAL DIFFRACTION PATTERNS

Rocking curves were taken for five different wave-length bands from 0.710 to 0.123A. The data are collected in Table III and the rocking curves are plotted in Fig. 12. Their extreme narrowness is remarkable. The curves are not entirely reproducible when various portions of the crystal plate are used. Variations as large as 30 percent may occur. This may account for the discrepancy between the points above 0.25A taken with the molybdenum tube. The smallest incremental setting available was $\frac{1}{4}$-second of arc. Some of the patterns were so narrow that difficulty was experienced in obtaining good profiles. Figure 13 is a log-log plot of the data given in Table III. Where boxes are shown about the experimental points, these represent both the wave-length band and the probable errors of intensity to be associated with each point. The theoretical curves are calculated on the assumption that the crystals are ideally perfect.

DISCUSSION OF RESULTS

The first result which can be deduced from these observations on stressed and unstressed quartz is that the unstressed crystalline quartz behaves more nearly like a perfect crystal than does the bent crystal. The integrated reflection coefficient for the flat specimen falls off certainly less rapidly than λ while for the bent crystal it falls off as λ^2. For the flat crystal, the behavior of $P(0)\exp[\mu_0 t_0/\gamma_0]$ and W_θ is in qualitative agreement with what one might expect if the specimen were nearly but not completely perfect.

¶¶ The parallelism of the internal (310) planes of the quartz slab (which exhibit no cleavage or other developed faces) with the axis of rotation of the pivot was established first by photographing the reflections from both sides of the planes of crystal *B* at a distance of 100 cm and adjusting the crystal on its support till these images occurred at the same height. The final fine adjustment was made so as to yield the narrowest possible parallel rocking curve.

Let us consider an almost perfect crystal in which there exist domains over which the lattice is perfect. Assume, however, that these domains are not perfectly oriented in the macroscopic crystal, but are randomly rotated relative to one another through *very small* angles. If very long wave-length radiation is scattered by this crystal, it can appear to behave as a perfect crystal only so long as the slight angular misorientation is small compared with the diffraction pattern width. Reference to Table I shows that the width w of a perfect crystal pattern varies as λ to the first power. The effect of absorption will be neglected throughout this discussion. The integrated reflection coefficient R_θ and half-width w for this perfect case decrease linearly with λ. The peak of the single crystal Laue diffraction pattern for this case will remain constant (at 50 percent, as we have already shown).

As the wave-length decreases, the case we have just outlined is the first of three cases which we may distinguish in order as follows:

Case I. Angular misorientation η of the mosaic domains is small compared to the single-crystal diffraction pattern width, w. Ideal crystal extinction distance t_x small in comparison to domain size t_0. For this case, w should be proportional to λ, $P(0)$ the peak reflection coefficient should stay constant at 50 percent and R_θ the integrated reflection coefficient should be given by $\frac{1}{2}\pi w$ (witch-like diffraction pattern).

Case II. As the wave-length decreases the ideal single crystal diffraction pattern width w decreases proportionally thereto until w becomes much smaller than η the mosaic misorientation parameter. Also, with decrease in wave-length λ the ideal crystal extinction distance t_x *increases* in inverse proportion to λ. (This can be seen by referring back to Eq. (2) which takes the form $t_x \cong [r_0(|F_H|/V)K\lambda]^{-1}$, if we substitute λ for $2d\sin\theta$ and recall that $\cos\theta$ is essentially unity for the small angles here involved.) For case II, however, we shall assume that t_x has still not increased to the point where it is larger than t_0, the size of the mosaic domains.

For this case, w the diffraction pattern width should remain constant but because of the mosaic misorientation it should of course be broader than the ideal single crystal diffraction pattern width, w, for the same wave-length. $P(0)$, the peak reflection coefficient of the diffraction pattern, should stay constant at the value 50 percent. R_θ the integrated reflection coefficient should be greater than it would be for an ideally perfect crystal (because of the broadening of the pattern).

Case III. As the wave-length decreases still more, we come to the case where both the inequalities $\eta \gg w$ and $t_x > t_0$ hold so that now complete extinction does not occur in any of the domains.

For this case we shall tend to have w the width of the diffraction pattern constant (since it is now fixed by the mosaic misorientation) but the peak reflection coefficient $P(0)$ should diminish as λ^2 because the amplitude which is scattered will vary as λ. Since the pattern width remains constant R_θ should also vary as λ^2.

With ever-decreasing wave-length this λ^2 behavior is then the terminal behavior for the mosaic crystal. In an ideally perfect crystal, on the other hand, the transition between $R_\theta \sim \lambda$ and $R_\theta \sim \lambda^2$ would take place only when the extinction distance became comparable with the total plate thickness. But, in this case also the λ^2 behavior is the terminal behavior at short wave-lengths.

In Fig. 10, the dashed curve, A, represents the theoretical behavior of a mosaic crystal. Curve B represents theoretically the behavior of a perfect crystal. All crystal models should approach in behavior the curve A below the junction P because below this wave-length the extinction distance is greater than the plate thickness. It is of interest to note that in the region of about 500 x-units the observed integrated reflection coefficient for the bent crystal is about twenty times what the theory for a perfect crystal (curve B) would predict. This is in accord with results privately communicated to us which were obtained by B. E. Warren, at M.I.T.

The diffraction pattern width w should vary as λ down to wave-lengths corresponding to the junction P in a perfect crystal and then show a constant width. If the crystal is imperfect, the transition from the linear behavior with wave-length should take place at longer wave-lengths (transition between cases I and II) and the width should tend to become constant at greater widths. It was impossible to obtain any information on w for the bent crystal case except at 30 x.u. where the width of the diffraction pattern appears to be of the order of 5 sec. of arc.

The results obtained for unstressed quartz are in qualitative agreement with Parratt's finding for the (110) planes.[18] There remains a slight uncertainty concerning the effect of the unetched surface layers. The extremely narrow two-crystal rocking curves indicate their effect to be small however. Also, there has never been any indication that they contribute appreciably to the scattering in the two-meter curved-crystal case.

For the unstressed crystals, the wave-length range 0.12 to 0.71A of this study may quite possibly represent the transition from case I to case II mentioned where the ideal crystal diffraction pattern width just becomes comparable with the angular misorientation η. Here the diffraction pattern width w will remain constant but the peak reflection coefficient $P(0)$ will start to diminish slowly with diminishing λ in preparation for its eventual behavior proportional to λ^2.

In the case of the elastically curved crystal, the observed R_θ behavior (Fig. 10) *over the entire wave-length range from 500 x units to nine x units* is like that of the predicted terminal behavior at short wave-lengths for either an ideally perfect or a mosaic crystal.

We have as yet no good explanation for this behavior

[18] L. G. Parratt, Rev. Sci. Inst. **5**, 395 (1934).

of the curved-quartz crystals when used in the focusing gamma-ray spectrometer. It seems very unlikely that bending the quartz plate creates permanent misorientation of mosaic blocks in the way in which this is supposed to occur when a rocksalt crystal for example is bent. In fact, we have no evidence that the quartz undergoes any permanent change either in its macroscopic geometry or otherwise as a result of bending. The quartz might, however, become mosaic-like in structure in some elastically reversible way not now understood. Such a division into mosaic domains when under stress could be either by reason of misorientation between domains or by reason of translational displacements between domains of such a nature as to destroy the coherence of the reflections from adjacent domains. Unfortunately, it is very difficult to study reliably such things as the width of the two-crystal spectrometer parallel rocking pattern utilizing a curved crystal for either of the specimens because this would require a beam so narrow that the arc of curvature of the plate over the region of reflection would be less in angular measure than the intrinsic diffraction pattern width, a matter of a second or so of arc only. At the very short gamma-ray wave-lengths studied here, it would be next to impossible to get sufficient intensity to work with the two-crystal spectrometer even with flat crystals and broad beams.

APPENDIX

The authors are indebted to the editors of the *Physical Review* whose remarks have brought out the need for further clarifying certain points in the description of our method of measuring the integrated reflection coefficients, R_θ, by means of the two-meter focusing curved-crystal spectrometer. One editorial remark was that we had made no attempt in our theoretical treatment of the problem to take into account *the effect of the bending of the crystal lattice on the reflection coefficient.* Now this criticism is, in the strict sense, *true.* We are as yet unable to formulate a rigorous *dynamical* theory of x-ray reflection for a curved lattice. Obviously all the well-recognized methods of attack (depending for example on Ewald's reciprocal lattice representation) break down because we no longer have to do with a strictly periodic structure. But we suspect that the editors (and, hence, probably many readers also) may have, as a result of reading the foregoing paper, erroneously imagined a much grosser defect than the lack of a rigorous dynamical theory for bent lattices. This is revealed by the next editorial remark to the effect that a beam of x-rays scattered in one layer of such a bent crystal slab can only go a certain distance before it encounters planes of different orientation (because of the bending) which therefore fail to satisfy the Bragg condition for the wave-length in question. Thus, it is asserted, the distance over which reflection is possible will be limited. This, it is stated, would be a direct effect of the bending which would tend to increase R_θ.

This argument we believe overlooks the fact that for source points on the focal circle of the instrument (when used as ours is in transmission), *the bending stresses change the lattice constant of the crystal in exactly the right manner through its thickness as to nullify the above supposed effect.* Y. Cauchois was the first to point out that on the convex side of the bent crystal slab, the grating constant (for the planes normal to the slab and parallel to the cylindrical generators) is increased by the tension in that region so that the Bragg angle for reflection is *decreased* while on the concave side the reverse is true. It is easy to prove that so long as Bernoulli's assumption for the bending of beams applies (that initially plane sections remain plane after bending) this effect will be just such that *rays emanating from one and the same point on the focal circle will encounter the crystal slab so as to satisfy the Bragg condition at all points throughout its entire thickness for one and the same wave-length.* As far as the geometrical optics of the selective reflection is concerned (ignoring multiple reflections to-and-fro between planes), the case seems thus to be beyond criticism. We propose to show here that this holds even for to-and-fro reflections. It is true of course that in our instrument an extremely minute and easily calculable aberration exists* because the design is of the approximate focusing type. This effect is

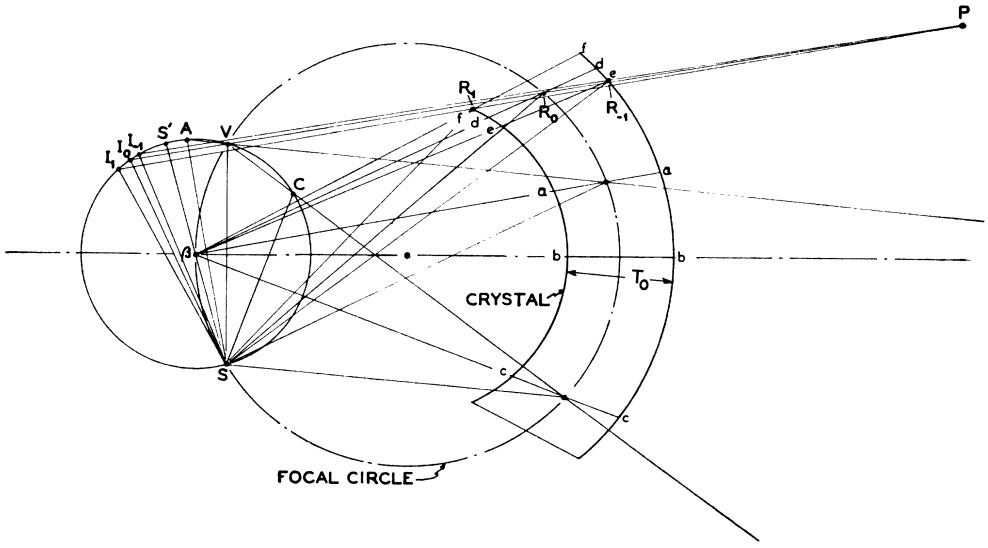

FIG. 14. To illustrate the reflection points R_1, R_0, R_{-1} and the corresponding images I_1, I_0, I_{-1} of the source point S mirrored in three different lattice planes of the curved crystal for a fixed observation point P. For simplicity the "exact" rather than the approximate focusing type of crystal is shown, a change which introduces no modification in the principles to be illustrated.

* See Fig. 3 and related text in our paper, Rev. Sci. Inst. 18, 629 (1947).

however far smaller even than the perfection of focusing we have so far been able to attain with our best curved-crystal holder would permit us to detect. All such minor effects are completely taken into account in our method of reducing our data (see Fig. 8 and related text for a summary of the factors involved in translating the observed quantity Γ_i into the desired reflection coefficient R_θ).

We have in a geometrical sense made a certain start in the direction of a more rigorous treatment of diffraction (by an accurately bent ideal crystal) which seems to indicate that the effect of such bending in limiting the domain of coherent interference in the crystal lattice must be practically quite beyond detection. In Fig. 14 the thickness T_0 of the bent crystal slab is enormously exaggerated relative to the radius of curvature for better clarity. The Bragg angle is also exaggerated for the same reason and for simplicity the exact focusing instrument is the one shown (neutral axis of the bent slab coinciding with the focal circle). The source is at S and the virtual focus for the selectively reflected rays leaving the crystal is at V. β is the convergence point of the reflecting crystal planes. Let us construct the image points of the source S for reflection by different atomic planes in the bent crystal. Simple geometrical considerations show that for the plane *bb*, which coincides with a diameter of the focal circle, the image of S is at V. For other crystal planes, such as *aa* or *cc*, the images of S lie in various positions such as A or C on the *circle* $SCVAS'$ whose center is at β, whose radius is βS, and whose diameter is $S\beta S'$. We shall call this circle the *image circle*. We are to think then of an arc of this circle (such as AC) as being closely studded with the image points of S mirrored in each and every one of the atomic lattice planes of the bent crystal slab. The lines SC and SA are the normals to the crystal planes projected from S. Furthermore, this geometry makes it clear that the multitude of image points of S mirrored in all the reflecting lattice planes of the curved crystal *are equidistantly spaced along that arc*. None of the geometrical results so far stated *involve any approximation whatever*. They are rigorous.

For the symmetrical Laue reflection of this type, as already pointed out in the preceding text, the very slight refractive bending of the rays at the entry and exit faces of the slab is just compensated by the change in wave-length inside the slab so that externally everything takes place as though the refractive index were strictly unity. It seems reasonable therefore to assume that the interference effects which will decide the intensity of the reflected beam leaving the convex side of the crystal will be essentially the same as though the crystal were removed and a multitude of coherent and equidistant sources studded along the arc AC were substituted for it. (This argument, for the moment, ignores multiple to-and-fro reflections in the crystal.) It is interesting to note how very different this set of virtual source points is from the set which would be observed *if the crystal were not bent*. For an unstressed crystal, the image points lie on a straight line, the common normal dropped from S to all of the (projected) lattice planes. Thus, the loci of images for the stressed and unstressed crystals lie roughly at right angles to each other. For the unstressed crystal the spacing between adjacent image points on the straight locus is $2d$ where d is the crystal grating space. For the curved crystal the spacing between adjacent image points on the circular arc AC can readily be shown to be $2d\sin\theta = n\lambda_B$ where d is the unstressed grating space, n is the order of reflection used (in all of our studies $n=1$) and λ_B is the wave-length satisfying the Bragg condition for reflection at angle θ.

Let us now consider classically how the rays actually interfere (constructively or destructively) so as to produce Bragg selective reflection in our curved crystal. Obviously we are dealing here with Fresnel rather than Fraunhofer diffraction. In order that reflections from a number of different atomic planes may cooperate coherently, it is necessary that rays starting from a source point S (an emitting atom), after reflection on different planes, shall, by different paths, eventually reunite at an observation point P (an absorbing atom in the detecting system). The "interference" (superposition of wavelets) *does not in reality occur in the crystal* but at the point of observation P. Neither S nor P are at infinity.

Let us consider how to construct the different rays arriving at P from different atomic mirror planes in the curved crystal. Clearly the fact that these mirror planes have *limited extension* (because of the limited thickness T_0 of the bent crystal slab) greatly restricts the number of such planes that can co-operate to send rays from S to any one given point P. Each plane will have one and only one geometrical reflection point R_i† for the given source and image points S and P. That mirror plane *dd* for which the geometrical reflection point R_0 *lies on the focal circle* (there can be not more than one such plane for specified positions of S and P) will furnish a ray to P directed as though it came from V. It will in general however *not* have V as its *image point*. The point I_0 where the line VP (or its extension) cuts the image circle again will be the image point. Now for other mirror planes such as *ee* or *ff* adjacent to the plane just referred to, the geometrical reflection points R_1 or R_{-1} will lie either inside or outside the focal circle and the corresponding image points from which the rays appear to arrive at P will be located as at I_1 or I_{-1} on a short arc of the image circle on either side of the point I_0. The range of image points I_i and geometrical reflection points R_i which can be operative to send rays to P is limited then by the thickness of the crystal slab, for when the reflection point R_i no longer lies inside the slab, reflection no longer occurs. The small range of different Bragg angles covered in this way corresponds to the above mentioned variation in grating constant as we pass through the thickness of the crystal slab resulting from the varying degrees of strain which the bending stress has set up on either side of the neutral axis. We have, of course, here selected a very exaggerated lateral position for P on purpose to clarify the geometry and as already stated the thickness of the crystal slab and other geometrical magnitudes such as the Bragg angle are also greatly exaggerated for the same reason. Clearly, however, in this idealized geometrical optical treatment the only specific effect of the bending which could place a limitation on the number of mirror planes cooperating coherently in sending wavelets to P *must come from the curvature of the short arc such as* I_1I_{-1} *on which the uniformly spaced image points lie* because this is the only effect of bending the crystal which introduces any important inhomogeneity in the otherwise uniformly increasing sequence of path lengths measured from the various image points I_i to P. Very simple considerations suffice to convince one that in the real geometry of our two-meter instrument the limited thickness of the crystal slab causes the number of image points clustering around I_0 to be far too limited to permit the accumulation of a phase change of order π through the curvature of the image locus. An order of magnitude for the number of co-operating image points can be found by computing how many planes a straight ray incident at the Bragg angle θ must cross in traversing the thickness of the unstressed slab. This is $T_0\tan\theta/d$ and in our two-meter instrument with a 1-mm thick crystal slab, for $\lambda = 8$ x.u. is about equal to 4×10^4. If we consider (see Fig. 15) the short arc of the image circle (on which the image points are clustered about I_0 with uniform spacing λ), then the projections of these image points on the ray direction furnish a means of closely approximating the successive path differences for the different paths I_iP. The angle α_0 between the image arc at I_0 and the ray direction can be approximated as x/D where x is the distance from the center of the curved crystal to the region in the crystal at which the reflection is occurring and D is the diameter of the focal circle. The difference of optical path for any

† As C. G. Darwin has pointed out in his remarkable early papers in 1914 on the dynamical theory of x-ray reflection, a reflection point such as R_i is in reality the center of a system of elliptical Fresnel zones, laid out on the atomic lattice plane and the explanation of the mirror reflection in terms of classical physical optics involves the coherent co-operative scattering of the entire pattern of atoms studded over these Fresnel zones which are the loci of points of equal path difference. C. G. Darwin, Phil. Mag. **27**, 325; 675 (1914).

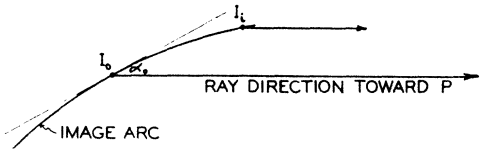

FIG. 15. To illustrate the geometry involved in the derivation of the dephasing of the interference from the array of images I_0 to I_i, by reason of the curvature of the locus on which they lie.

two image points on the arc will be $\lambda\cos\alpha$ where α is the angle with the ray direction at that point on the arc. Relative to the path I_0P the cumulative path difference δ_i for any image point I_i is found to be

$$\delta_i=\lambda[\cos\alpha_0+\cos(\alpha_0+\mu)+\cos(\alpha_0+2\mu)\cdots\cos(\alpha_0+i\mu)],$$

where $\mu=2d/D$ is the angular change in the direction of the image arc between adjacent image points. On the other hand, the cumulative path difference δ_i' if the image point locus had been a *straight* tangent to the arc at I_0 would have been

$$\delta_i'=\lambda i\cos\alpha_0.$$

By expanding the cosine terms in the expression for δ_i, the difference $\delta_i-\delta_i'$ can be readily shown to be

$$|\delta_i-\delta_i'|=\lambda i^2 d\sin\alpha_0/D.$$

This formula permits us to compute how many image points i must be included before $|\delta_i-\delta_i'|$ amounts to the order of a whole wave-length λ. The requisite number i_p is $i_p=D^{\frac{1}{2}}/(d\sin\alpha_0)^{\frac{1}{2}}$ or since α_0 is small and can be approximated by x/D we can write

$$i_p\cong D/(xd)^{\frac{1}{2}}.$$

For our two-meter spectrometer and with $x=4$ cm, $i_p=10^6$. Thus, 25 times as many image points are required (before dephasing from curvature becomes important) than the number actually available. The value of $\cos\alpha_0$ for our assumed case turns out to differ from unity by about $2\cdot10^{-4}$.

Now, in order to include in our discussion the case of repeated to-and-fro reflections between lattice planes in the crystal, we must consider not only the primary image points I_i (which we shall now distinguish as *primary* by calling them I_i') but also the images of these images I_{ij}'' each mirrored in an appropriately selected restricted set of atomic planes, the tertiary images I_{ijk}''' of each of these in turn mirrored in another appropriately selected restricted set of planes, etc.,‡ obviously only primary, tertiary, quinary and in general the images of *odd* ordinal number, I_i', I_{ijk}''', I_{ijklm}''''', etc. (lying on the same side of the central axis, $b\beta$, as the point V), operate as coherent image points to determine the intensity at P. Now a little thought will convince the reader *that all image points*, whether they be primary, secondary, tertiary, or of whatever ordinal number, *lie somewhere on the image circle*. Furthermore, it is not difficult to prove that all the cooperating image points *of odd ordinal number* lie at points on the image circle which belong to the same set as the primary image points, namely the set (of which I_0' is a member) consisting of points uniformly spaced along the arc with constant angular spacing μ between adjacent points. Thus, what we have proved for the primary image points (that the dephasing from curvature of the locus is negligible) will be equally true for the image points of higher ordinal number and in fact these will in general not lie as remote from I_0 as extreme members of the primary set for it can be shown that the sum of all subscripts without regard to algebraic signs,¶ $|i|+|j|+|k|\cdots$ for a given higher (odd) ordinal image point must have an upper bound of order of magnitude $T_0\tan\theta/d$ (or approximately $10^7\tan\theta$ in our instrument) whereas, for a higher odd ordinal image, the most remote position on the image arc from the origin I_0 will be given merely by the sum of the *alternate* subscript numbers $|i|+|k|\cdots$ (with the subscript numbers for the even ordinal reflections omitted from the summation). We arrive then at the conclusion *which holds rigorously, either for primary reflections or higher ordinal to-and-fro reflection in the crystal, that the dephasing effect of locus curvature cannot place a limit on the number of planes which cooperate coherently*. This holds for an ideally perfect crystal slab ideally bent so that its atomic planes pass through a common point β, so long as the lateral position of the observation point P from the central axis of the instrument defines an angle $\alpha_0\cong x/D$ as small as we have in our two-meter spectrometer. The conclusion seems inescapable that, for the ideal crystal case as stated, the above limitation must be placed by the thickness T_0 of the slab only.

‡ Each subscript after the first indicates the number of atomic planes traversed between two successive reflections.

¶ Note that, save for the first subscript, i, which may be either positive or negative, the series of subscripts, j, k, $l\cdots$, must have terms whose algebraic signs alternate because of the to-and-fro reflection.